25th ABCM International Congress of Mechanical Engineering
October 20-25, 2019, Uberlândia, MG, Brazil

HYDRODYNAMIC AND STRUCTURAL DESIGN AND ANALYSIS OF AN IMPELLER FOR A CAVITATION TUNNEL

Ricardo Sbragio
Manassés do Nascimento Monteiro
Eduardo Ribeiro Malta
Diretoria de Desenvolvimento Nuclear da Marinha - Av. Prof. Lineu Prestes, 2468 - Cidade Universitária - São Paulo - SP
e-mail: sbragio@marinha.mil.br

Abstract. *The objective of this paper is to present the design and the analysis of an impeller for a cavitation tunnel. The impeller design uses circulation theory to determine the thrust needed to overcome the head loss of the cavitation tunnel and the associated torque. The structural design determines the stress at the impeller blade using beam theory. In order to check the design results, a Computational Fluid Dynamics (CFD) and a Finite Element Method (FEM) analysis are done. The CFD mesh is divided in a rotating mesh at the impeller blades and a static mesh for the rest of the cavitation tunnel domain. The maximum impeller rotation is set to be the input. The velocity at the cavitation tunnel is obtained as the result of the analysis. The pressure distribution over the blade obtained from CFD is used for FEM structural analysis. The final velocity at the test section for the design rotation and the Von Mises stress at the impeller blades agreed well with the design values.*

Keywords: *Cavitation Tunnel, CFD, FEM, Impeller, Hydrodynamics*

1. INTRODUCTION

The Hydrodynamic Laboratory (LABHIDRO) operates a Small Cavitation Tunnel (SCT). This facility has a test section of 215mm x 215mm, where small wing sections can be tested. However, the main purpose of this facility is to conduct hydroacoustic tests with impellers in order to consolidate the design procedures that are going to be used in the impeller design of the Large Cavitation Tunnel (LCT). The SCT hydrodynamic and acoustic characteristics were discussed in paper (Barnack Neto et al., 2017). Figure 1 shows a picture of the SCT.

Figure 1. LABHIDRO's Small Cavitation Tunnel.

The SCT is a closed loop with an impeller in the lower part. In the upper part, the test section is located after the contraction and before the main diffuser. Under the test section, there is an acoustic trough equipped with a hydrophone. The maximum design velocity at the test section is 6 m/s and corresponds to a rotation of 300 RPM in the impeller. The impeller that is in operation up to now was designed with 4 blades (without skew) and has a stator with 9 fixed blades.

In the paper (Barnack Neto et al., 2017), the influence of the blade pass frequency of the rotor/stator setup was discussed. At a specific rotation velocity of the impeller (209 RPM), acoustic peaks were identified, caused by a coincidence frequency with the tunnel geometry. The peaks correspond to the blade pass frequency shown in Eq. 1.

$$f = N_r N_s n N_{harm}/60 \quad (1)$$

Where f is the acoustic response frequency (Hz); N_r is the rotor number of blades; N_s is the stator number of blades; n is the impeller rotation in rpm; and N_{harm} is the harmonic number.

As the future LCT needs to be as quiet as possible, due to its hydroacoustic measurement requirements in the test section, a new impeller is designed to the SCT facility, with the objective of testing the design procedures and reducing the emitted noise. This new impeller has a higher number of rotating blades and a high skew angle. The increase of the number of blades, together with the use of a high skew angle are an efficient way to reduce the vibrations originated by the blade operation in the wake field at the impeller section and the vibrations caused by the blade pass frequency. In this paper, this new impeller design is presented, together with its CFD hydrodynamic performance analysis and its FEM structural resistance analysis.

The structure of this paper is as follows: This first section is an introduction with the objective of this paper. The second section describes the head loss determination in the SCT. The third section describes the impeller design using circulation theory and the analytical analysis that were done during the project phase for determining the best configuration of the impeller, regarding the number of blades and skew angle (structural resistance and vibration). Section 4 shows the CFD hydrodynamic analysis. Section 5 presents the FEM structural analysis. The conclusion is presented in Section 6. Sections 7 and 8 show respectively the acknowledgements and the references.

2. HEAD LOSS AT SCT

The head loss calculation defines the thrust that the impeller shall provide to reach the design speed of 6m/s at the test section. The SCT is divided in 19 sections, which are shown in Fig. 2. The head loss is calculated in each section based on the theory and tables presented in the work of Idelchik (1986).

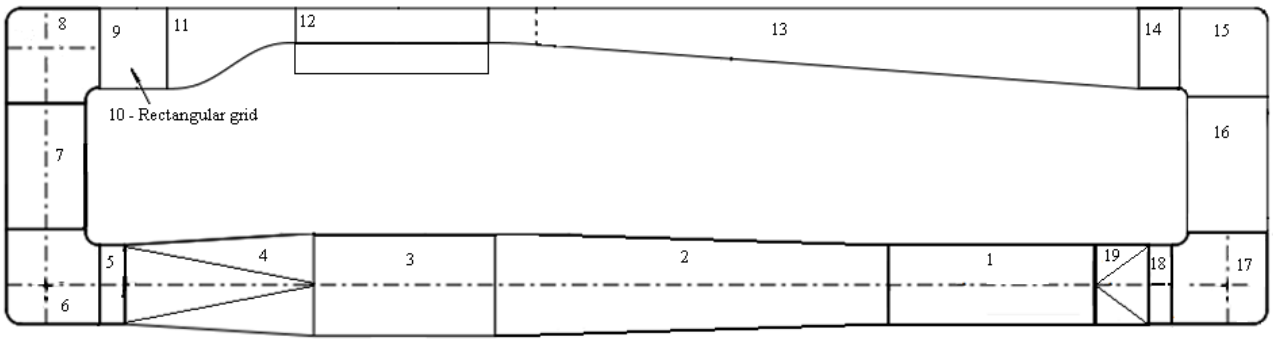

Figure 2. SCT sections for head loss calculations.

The impeller is placed in section 1 and has the configuration shown in Fig. 3.

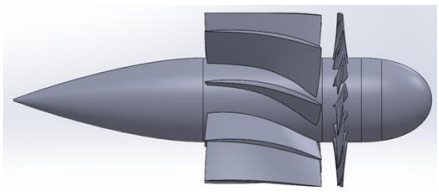

Figure 3. Impeller configuration.

Table 1 shows the models that were used in the determination of the head loss at each section. In the sections where no exact model was available (for example: impeller and square cross section contraction), the simulation considered the most similar models presented in Idelchik (1986).

Table 1. Models used in the head loss calculation.

Section	Section name	Head loss model (Idelchik, 1986)
1	Impeller section	Impeller was modeled as a convergent nozzle of circular cross section, a circular concentric annulus and a conical diffuser.
2	Lower diffuser	Conical diffuser
3	Resorber	Circular tube with rough walls
4	Contraction (circular to square)	Transition from rectangular to circular cross sections
5	Junction	Tubes of rectangular and other types of cross sections
6	Elbow with turning vanes	Elbows and turns of rectangular cross sections with guide vanes
7	Ascending leg	Tubes of rectangular and other types of cross sections
8	Elbow with turning vanes	Elbows and turns of rectangular cross sections with guide vanes
9	Plenum	Tubes of rectangular and other types of cross sections
10	Rectangular grid	Grid made of thickened laths
11	Contraction	Converging nozzle of circular cross section (hydraulic diameter was used for the square cross section)
12	Test section	Tubes of rectangular and other types of cross sections
13	Diffuser	Diffuser of rectangular cross section
14	Junction	Tubes of rectangular and other types of cross sections
15	Elbow with turning vanes	Elbows and turns of rectangular cross sections with guide vanes
16	Descending leg	Tubes of rectangular and other types of cross sections
17	Elbow with turning vanes	Elbows and turns of rectangular cross sections with guide vanes
18	Junction	Tubes of rectangular and other types of cross sections
19	Contraction (square to circular)	Transition from rectangular to circular cross sections

The fluid properties are shown in Table 2.

Table 2. Fluid properties.

Properties	Value	Reference
Density (at 23°C)	997.5414 kg/m^3	ITTC, 2011
Viscosity (at 23°C)	0.93442e-6 m^2/s	ITTC, 2011

The head loss totalizes 6219.6 Pa at the maximum design speed of 6m/s.

3. IMPELLER DESIGN

3.1 Impeller blades design

The circulation theory approach is used for the hydrodynamic design of the impeller blades. The following assumptions apply:

a) The absolute flow velocity that enters the impeller is axial, without rotation;
b) The flow velocity relative to the impeller blade at the trailing edge is tangential;
c) The pump operates in a closed loop. There is no acceleration of the flow in the axial direction; and
d) The flow particles at the impeller blades move along a cylindrical path of constant radius. Hence, circumferential velocity of the particles does not change through its path at the impeller.

From these assumptions, the Euler´s equation for turbo machinery leads to:

$$\frac{H_{SCT}}{\eta} = \frac{u\, v_{u2}}{g}, \tag{2}$$

where H_{SCT} is the SCT head loss, which is increased by the hydraulic efficiency η to obtain the total impeller head loss, g is the acceleration of gravity, u is the peripheral rotation velocity of the blade and v_{u2} is the peripheral component of the absolute velocity of the flow at the trailing edge, as shown in Fig.4. Equation 2 allows obtaining the velocity component v_{u2}, by setting an initial value of η, which is iteratively adjusted during the design calculations. The other symbols used in the velocity diagram of Fig. 4 are the absolute inflow and outflow velocities at the impeller v_1 and v_2, the relative inflow and outflow velocities w_1 and w_2 and the flow angles α_1, α_2, β_1 and β_2.

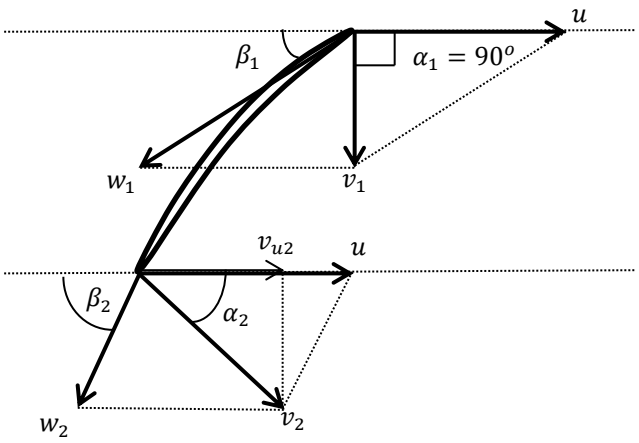

Figure 4. Velocity diagram at an impeller blade section at radius *r*.

The section lift and drag coefficients (C_L and C_D) relate to the section lift $\bar{L}$ and to the section viscous drag $\bar{D}$ generated by the blade (see Fig. 5) by Eq. 3 and Eq. 4, respectively.

$$C_L = \frac{\bar{L}}{0.5\rho\, c\, w_m^2} \tag{3}$$

$$C_D = \frac{\bar{D}}{0.5\rho\, c\, w_m^2} \tag{4}$$

where ρ is the fluid density, c is the section chord and w_m is the mean value of the relative flow velocity on the section. The relation between C_D and C_L is defined using angle λ, according to Eq. 5:

$$\tan\lambda = \frac{\bar{D}}{\bar{L}} = \frac{C_D}{C_L} \tag{5}$$

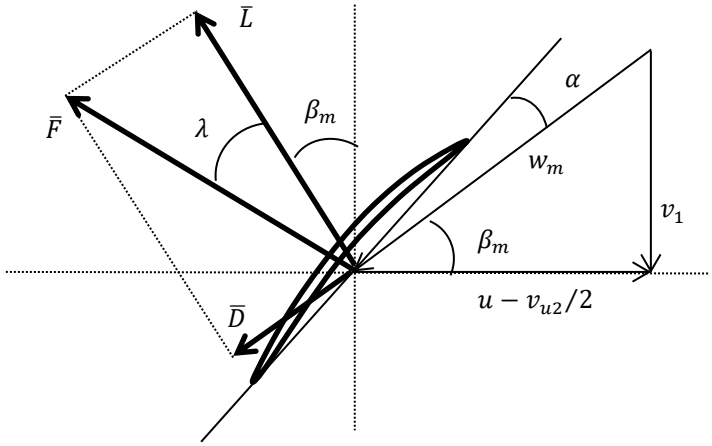

Figure 5. Forces on the impeller blade section.

The section lift coefficient C_L of the impeller blades is obtained by equaling the power needed to overcome the total impeller head loss to the power needed to rotate the impeller due to the section hydrodynamic lift and friction drag (Eq. 6):

$$\rho g \frac{H_{SCT}}{\eta} 2\pi r \eta_{vol} v_1 dr = z(\bar{L}\, sin\, \beta_m + \bar{D}\, cos\, \beta_m)\omega r dr \tag{6}$$

where η_{vol} is the volumetric coefficient that considers the loss of flow area due to the blade thickness, β_m is the mean value of the relative velocity angles and z is the number of blades.

Using Eq. 2 to Eq. 5 into Eq. 6 leads to:

$$C_L = \frac{4\pi}{z}\frac{r}{c}\eta_{vol}\frac{v_1 v_{u2}}{w_m^2}\frac{cos\lambda}{sin(\beta_m+\lambda)} \quad , \tag{7}$$

As the lift coefficient C_L is related to angle λ (Eq. 5), it appears on both sides of Eq. 7. Hence, this equation shall be solved iteratively.

The total thrust generated by the impeller is calculated by:

$$T = z\int_{r_h}^{R}(\bar{L}\cos\beta_m - \bar{D}\sin\beta_m)dr \tag{8}$$

where the blade radius r varies from the hub radius r_h to the tip radius R. The total thrust is also determined by:

$$T = H_{SCT}\,\pi(R^2 - {r_h}^2)\eta_{vol} \tag{9}$$

Equaling Eq. 8 and Eq. 9, allows obtaining the total thrust T and the hydraulic efficiency η, using an iteration scheme.

The section lift coefficient defines the camber of the blade section. The blade section thickness distribution chosen for the impeller is the NACA 66 (Mod), with a camber distribution NACA a = 0.8 (Brockett, 1966). This section profile thickness and camber distributions are very used in propeller design and have a good pressure distribution over its length, which is desirable for avoiding cavitation. The inflow angle of attack α is defined as the ideal angle of attack α_{id} of the section profile, which corresponds to a shock free inflow, also desirable for avoiding cavitation and separation at the leading edge. The NACA 66 (Mod) thickness distribution and the NACA a = 0.8 camber distribution have the lift coefficient and the ideal angle of attack determined by Eq. 10 and Eq. 11, respectively (Brockett, 1966):

$$C_L = 2\pi(1 - 0.83\tau)(\alpha + 2.05f)\,, \tag{10}$$

where τ is the thickness over chord relation, α is the angle of attack in rad, measured from the leading edge – trailing edge line and f is the maximum camber over chord relation. During the impeller design, the angle of attack α is set to be the ideal angle of attack (α_{id}), by using the following relation (Abbott et al., 1959), where $C_{L\,id}$ is the ideal lift coefficient:

$$\alpha_{id} = 1.54^o\frac{\pi}{180^o}C_{L\,id} \tag{11}$$

From Eq. 10 and Eq. 11, the camber associated with the shock free entrance can be obtained:

$$f = C_{L\,id}\left(\frac{1}{2\pi(1-0.83\tau)} - 1.54^o\frac{\pi}{180^o}\right)\frac{1}{2.05}\,, \tag{12}$$

The section lift coefficient that is needed to overcome the head loss, obtained from Eq. 7, is used in Eq. 12 to obtain the section camber. CFD analysis verified the hydrodynamic behavior of the impeller at maximum rotation speed, as shown in Section 4.

During the hydrodynamic design, structural analysis using beam theory was done, in order to obtain a suitable thickness and chord distributions. The impeller material is Aluminum 5052 with a yield stress of 65MPa, The thrust, tangential force and the centrifugal force were computed and the Von Mises criteria was used to obtain the equivalent stress. The operation condition for the stress calculation is the impeller operating with an overload of 10% in the rotation, which is 330 rpm and a correspondent test section velocity of 6.6m/s. The maximum Von Mises stress occurred at the pressure side near the impeller hub, which is 13 MPa, correspondent to a safety factor of 5. A post-project FEA analysis checked the stresses in the overload condition as presented in Section 5.

The number of blades and the skew angle were defined from vibration analysis, according to the estimated wake incident on the impeller. A configuration of 13 rotating blades and 9 stator blades was chosen. This configuration avoids a common divisor for the number of rotating blades and of stator blades, reducing vibrations, as only one rotating blade position coincides with one stator blade position during rotation. Using a large number of rotating blades also reduces the intensity of the harmonic of the wake multiple of the number of blades that induces vibrations. The impeller is designed with a skew angle of 50% at the blade tip (13.85°), which reduces the pressure intensity of the passage of the rotating blades over the stator. The final impeller geometry is shown in Fig. 6. Even with a large number of blades, there was no superposition of the rotating blades, which facilitates the manufacture.

The 13-bladed impeller has 0.529m diameter with 0.2561m hub diameter. There is a gap of 0.5mm between the blades and the carcass of the cavitation tunnel. It produces a design thrust of 962.9N and requires a torque of 77Nm and

a power of 2.42 kW at the maximum rotation of 300rpm. The design velocity at test section at this rotation is 6m/s. A permanent magnet motor is placed inside the impeller hub in a watertight case to drive the rotating blades.

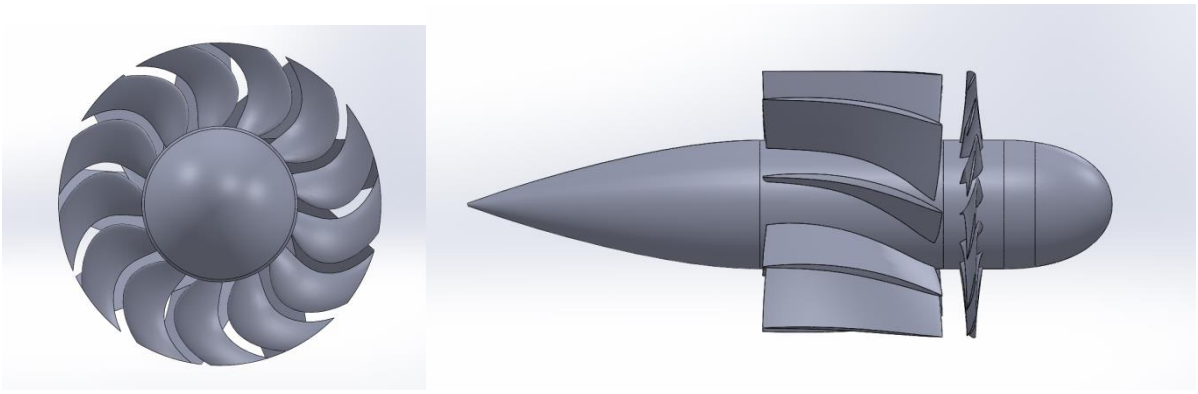

Figure 6. Impeller geometry.

The main impeller blade characteristics (chord, maximum thickness, skew angle, camber and pitch) are shown in Fig. 7.

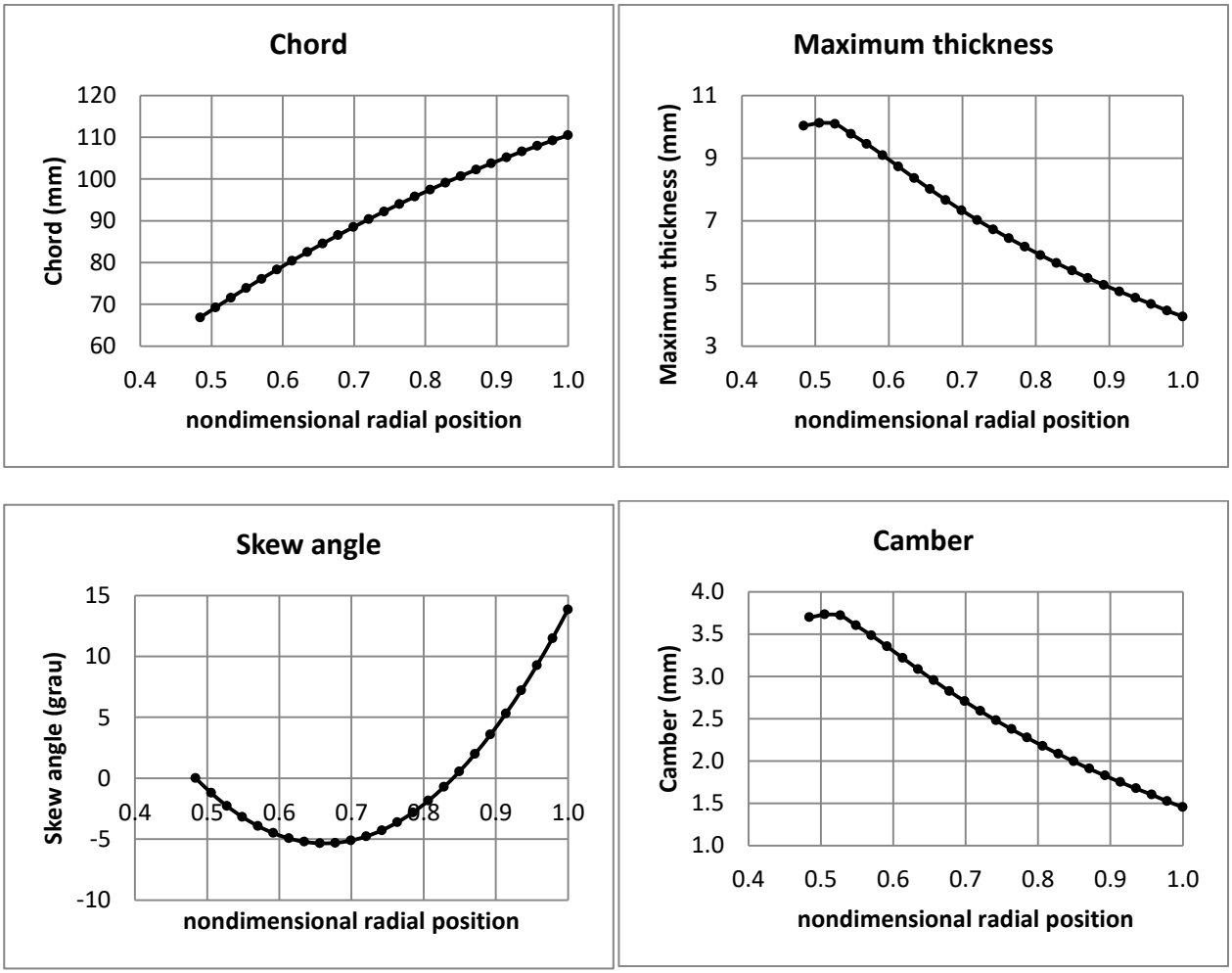

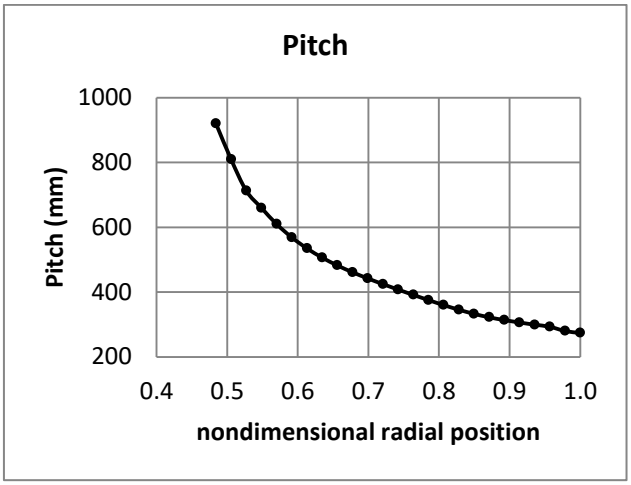

Figure 7.Main impeller blade characteristics.

3.2 Stator blades design

The stator design has the objective of reducing the flow rotation downstream of the rotating blades. The stator also holds the impeller inside the cavitation tunnel. As the impeller motor and thrust bearings are placed inside the impeller structure, the stator and its fixing bolts shall support all the hydrodynamic thrust and torque generated by the impeller.

The impeller design is quite simple. The inflow direction at the stator leading edge has the direction of the v_2 outflow absolute velocity of the stator blades. Small corrections can be applied in the inflow angle, based on empirical or in CFD analysis. The outflow angle can be set to be aligned to the axial flow, and can also be corrected by CFD analysis, if necessary. In the design of the stator, the camber was set to be of constant radius, with a smooth curvature in order to avoid separation or cavitation. The flow around the stator was analyzed in CFD and no separation was detected.

4. CFD HYDRODYNAMIC ANALYSIS

The CFD analysis uses software Ansys-CFX version 15.0 in order to obtain the torque, thrust and the velocity in the test section, for an impeller rotation of 300 rpm. Two domains are defined: a rotating domain at the impeller rotating blades region and a static domain for the rest of the cavitation tunnel.

The mesh uses tetrahedral elements far from the wall and prismatic elements close to it in order to capture the boundary layer. It comprises a total of 33.350.013 elements. The mesh of the whole fluid domain is shown in Fig. 8. The static and the rotating meshes at the impeller are shown in Fig. 9.

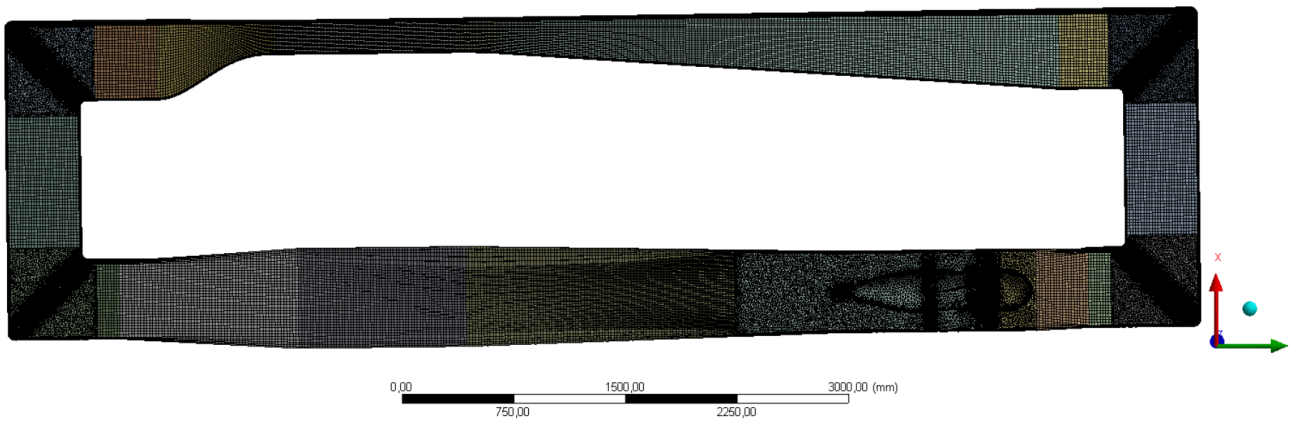

Figure 8. Mesh of the fluid domain.

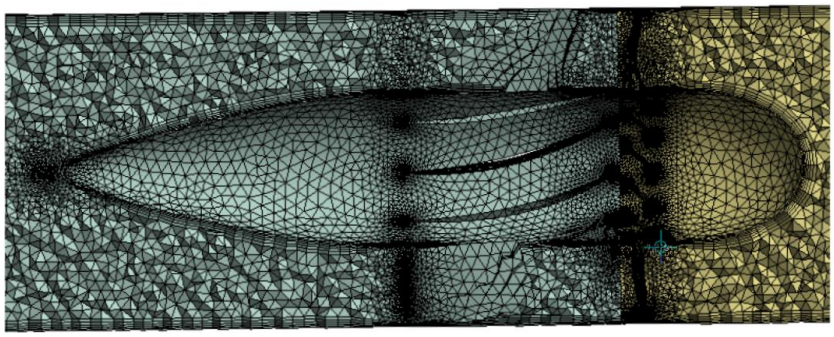

Figure 9.Static and rotating meshes at the impeller region.

The results from the CFD analysis are compared to the project results in Tab. 3 for a 300 rpm impeller rotation. Good agreement is obtained for the results.

Table 3. Comparison between the project and CFD analysis results.

Parameter	Project	CFD analysis
Mean velocity at the Test Section (m/s)	6	5.998
Impeller thrust (N)	962.9	963.9
Torque (Nm)	77	61.8

5. FEM STRUCTURAL ANALYSIS

The last verification step on the impeller design is the structural analysis. The original design process already estimates a value for the maximum blade stress using beam theory which is a quite simple, but fast design method. A series of assumptions are made for the analytical calculations. The impellers blades are short, compared to the overall diameter of the equipment. Its geometry is slick and a high skew gives it an irregular shape (Fig. 6). For that reason, it is not expected to have a uniform stress state with constant stresses in the cross section. Hence, a numerical finite element analysis is necessary, not as a design tool, but for verification purposes regarding the stress concentration levels on key regions, such as the base of the blade.

5.1 Mesh

The impeller geometry is quite challenging to map and mesh with the usual elements (tetrahedrons, hexahedrons, pyramids and wedges) due to the curvature on the leading edge and to the extremely thin and sharp trailing edges. It can be noticed in Fig. 10, that there is a high a concentration of elements on the leading and on the trailing edge. For the lesser critical regions, the elements were kept larger, in order to save some memory space.

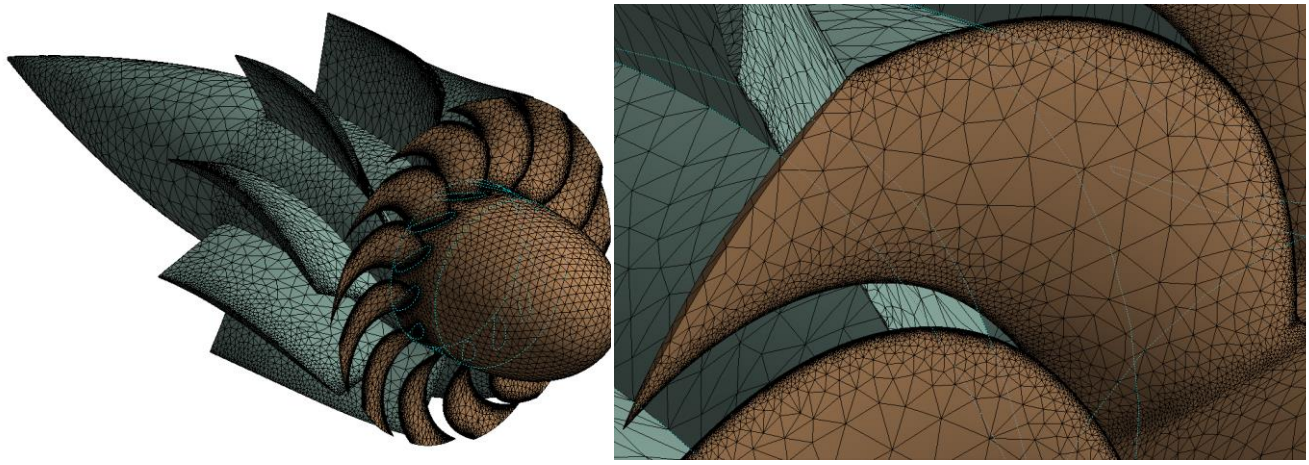

Figure 10. **Left**: impeller mesh for the structural analysis. **Right**: Detail for the mesh on one of the blades.

In total 3.269.890 nodes and 1.912.699 elements were employed in this analysis, which is considerably high. A face sizing of 0.5 mm was used on the impeller rotating blades. A general method control was imposed to all bodies, with the option "tetrahedrons" and patch independent. Also, the global sizing control was set with a high level of "relevance", implying in a very refined mesh. The elements used were second order tetrahedrons, guaranteeing a nonlinear stress state representation within the elements.

5.2 Loads and boundary conditions

A one way fluid structure interaction scheme is used. This means that an imported pressure load is added to all surfaces of both the fixed and the rotational parts of the impeller. A fixed support is applied to the fixed blades, serving as the boundary condition for the entire model and the rotational part is fixed to it through a bonded contact. Also, a 10% overloaded rotational velocity of 330 RPM is applied to the impeller, in the form of a kinematic rotational velocity. Since it is a static load, it does not rotate the propeller, instead, it creates a centripetal force on the blades, generating displacements and stresses. Figure 11 shows the rotational velocity and the fixed support on the left and the imported pressure from the CFD analysis on the right.

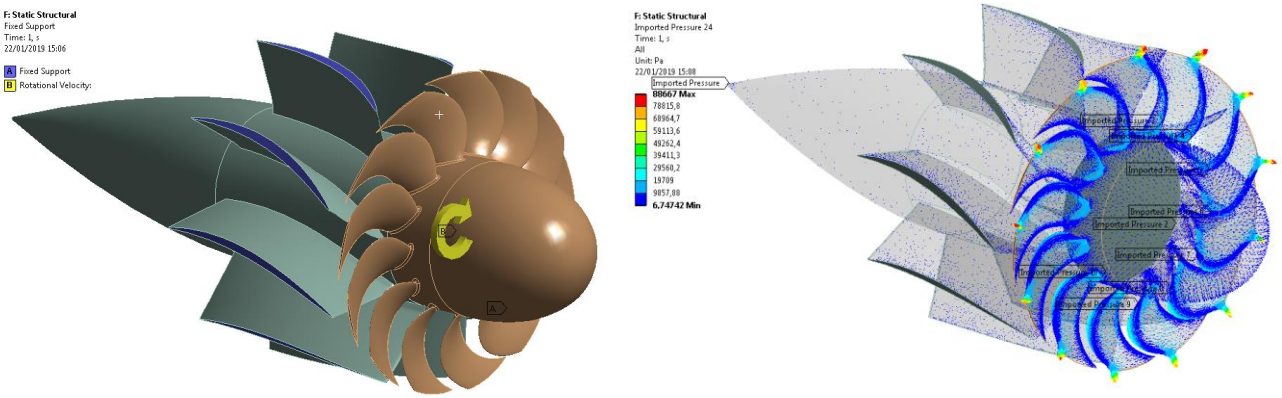

Figure 11. **Left**: Rotation velocity and fixed supports. **Right**: Vector representation of the imported pressure load.

5.3 Structural analysis results

The main result for the analysis was the stress on the propeller blades caused by the pressure and the rotation. Since the material used for all parts is Aluminum, a ductile material, the von Mises equivalent stress may be used instead of all other components. It can be seen in Fig. 12 that the stress state is quite similar for all blades and the values are higher on the rotating blades, more specifically, near the base, where the blade meets the hub. The maximum equivalent stress value was calculated as 12,93MPa. That value is substantially close to the 13 MPa provided by the beam theory model, showing that it can be a very good approximation.

It is also noticed that the stress state seems to form a pattern and repeat itself on every blade. This may naturally lead to a questioning on the need to model the entire propeller, and not a single blade section. The main reason for that is that the fluid pressure field that came from the CFD analysis is variable on the cross section. But this full model will surely become a valuable benchmark to evaluate future and simpler models.

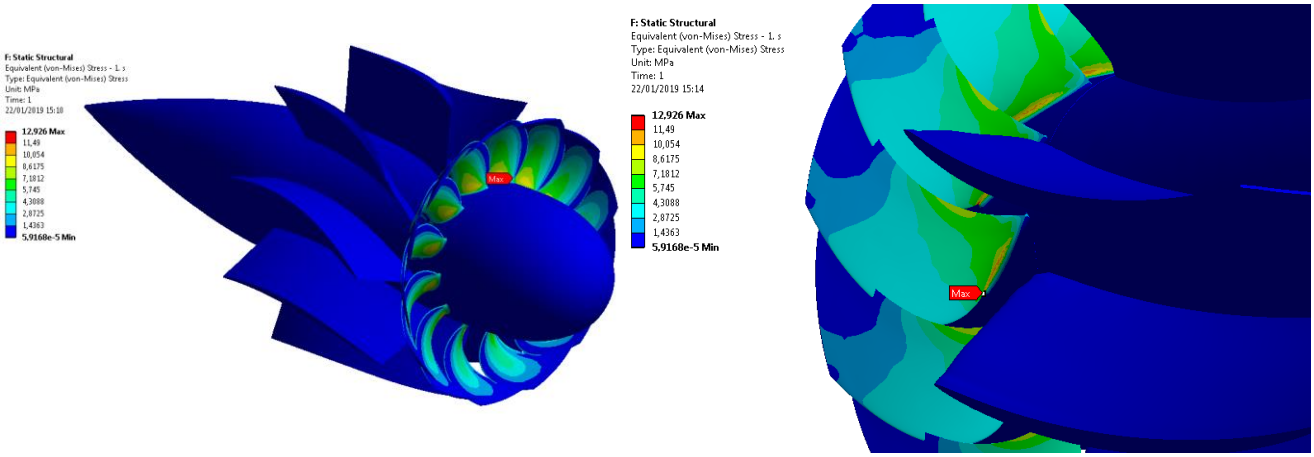

Figure 12. **Left**: Von Mises stress for the impeller. **Right**: Detail of the stress field near the base of the blade.

6. CONCLUSIONS

The circulation theory was used in the design of a new impeller for LABHIDRO's Small Cavitation Tunnel. The impeller was designed with a large number of blades in order to reduce the vibration and the noise originated by the blade pass frequency and by the wake incident on the impeller. The hydrodynamic and structural design results agree well with the CFD and FEM analysis of the impeller operating in the SCT. In the next steps, the impeller will be manufactured and tested in the SCT facility in order to confirm the design requirements and to validate the design methodology.

7. ACKNOWLEDGEMENTS

This work is supported by Diretoria de Desenvolvimento Nuclear da Marinha and by Centro Tecnológico da Marinha em São Paulo.

8. REFERENCES

Abbott, I.H. and von Doenhoff, A.E., 1959. *Theoty of Wing Sections*. Dover Publications, Inc, New York.

Barnack Neto, W., dos Santos Moura, A.J., Sbragio, R., da Silva Júnior, H.C. and Pansanato, L., 2017."Hydrodynamic and acoustic characteristics of LABHIDRO's Small Cavitation Tunnel". *In Proceedings of the 24th ABCM International Congress of Mechanical Engineering – COBEM 2017*. Curitiba, Brazil.

Brockett, T., 1966. *Minimum Pressure Envelopes for Modified NACA-66 Sectionswith NACA a = 0.8 Camber and BuShips Type I and Type II Sections*, Report n. 1780, David Taylor Model Basin, Bethesda, EUA.

Idelchik, I.E., 1986. *Handbook of Hydraulic Resistance*. Hemisphere Publishing Corporation, 2nd edition.

ITTC, 2011. *International Towing Tank Conference Recommended Procedures – Fresh Water and Seawater Properties*, Procedure 7.5-02-01-03, Revision 02, 2011.

9. RESPONSIBILITY NOTICE

The authors are the only responsible for the printed material included in this paper.